Journal of Information Systems and Telecommunication
Vol.13, No.4, October-December 2025, 266-277
http://jist.acecr.org
ISSN 2322-1437 / EISSN:2345-2773

Adaptive PID and Fuzzy Logic Control for Yaw Attitude in LEO Satellites

Stanley E. Ajagba[1], Udora N. Nwawelu[1], Bonaventure O. Ekengwu[1*], Nnaemeka C. Asiegbu[1], Dumtochukwu O. Oyeka[1], Ifeanyi M. Chinaeke-Ogbuka[1]

[1]. Department of Electronic and Computer Engineering, University of Nigeria, Nsukka, Enugu State, Nigeria

Received: 21 Oct 2024/ Revised: 04 Sep 2025/ Accepted: 29 Oct 2025

Abstract

The significance of an effective satellite attitude control system lies in its ability to ensure that data acquisition by a Low Earth Orbit (LEO) satellite is of good quality and reliable. In this paper, the design of an adaptive Proportional Integral Derivative (PID) controller and its modified form (PIDD), which includes an additional derivative component for a microsatellite y-axis attitude control system (ACS), is presented. Additionally, a Fuzzy Logic Controller (FLC) and its enhanced version, called Adjustable Gain Enhanced FLC (AGE-FLC), were designed. Models of the amplifier, actuator, and satellite structure were developed to derive the transfer function of the LEO satellite's yaw-axis attitude dynamics. Model Reference Adaptive Control (MRAC) based Proportional Integral Derivative (PID), referred to as MRAC-PID and its modified form, MRAC-PIDD, were designed. The models of the various control systems were developed in MATLAB and were used to simulate the designed control systems. The simulation results and analysis revealed that the MRAC-PID controller offered the most efficient performance in terms of fast response and transient time, with a rise time of 1.74 seconds and a settling time of 6.19 seconds. Also, the MRAC-PIDD and AGE-FLC exhibited no overshoot, indicating efficient performance in terms of stability and smoothness in torque control. All proposed control systems for the LEO satellite yaw-axis ACS met the performance criteria, except for the PID and FLC controllers, which yielded overshoots of 12% and 21.97%, respectively. Generally, it suffices to say that the introduction of the designed adaptive PID/PIDD controllers and the AGE-FLC enhanced the system performance.

Keywords: Adaptive PID; Attitude Control System; Fuzzy Logic Controller; LEO Satellite; Yaw-axis.

1- Introduction

Satellite attitude refers to the orientation of a satellite in space, taking into account various coordinate systems [1]. The importance of satellite attitude control is evident in various areas, extending beyond communication, navigation, and earth observation. For example, in a communication satellite, it ensures that the satellite antennas are aligned with the Earth or other satellites, enabling reliable communication. Also, it maintains optimal signal strength by keeping the antenna pointed in the correct direction. The satellite's orientation in space is controlled by satellite attitude control (SAC), which ensures proper control manoeuvring. However, the flight attitude of the satellite changes to different degrees during the on-orbit flight of a satellite because of external disturbances and gravitational perturbations [2]. These disturbances acting on the satellite can cause it to shift over time, and the effect can manifest as angular variations in pitch, yaw, and roll [3]. Given that a satellite is exposed to varying disturbances, maintaining a preset attitude and a specified attitude is crucial to achieving the desired function and performance criteria [4]. Hence, for a satellite to accomplish its tasks, it is crucial to examine its control subsystem and then select the control technique that ensures the achievement of attitude adjustment and stability by improving both transient and dynamic characteristics, as well as steady-state performance [4]. Since a satellite is subject to various disturbances in orbit, its attitude and its reliability regarding data acquisition are largely dependent on the effectiveness of the SAC system. Consequently, several techniques are presented in previous studies for accurate satellite operation control. Classical and linear control schemes such as Proportional Integral and Derivative (PID) control algorithms, are prevalent implemented methods. As an example, a PID controller was used to stabilize the yaw-axis of a microsatellite by minimizing the Integral Time Absolute Error (ITAE) criterion in [5]. Similarly, other approaches involving the use of PID and its enhanced approaches in achieving

✉ **Bonaventure O. Ekengwu**
bekengwu@yahoo.com

attitude control regarding satellite yaw-axis are well documented. The PID controller uses three simultaneously coordinated computational operations to carry out corrective commands that put the plant or process response in a new state [6]. In the control of plants or processes in industries, PID controllers have been the most applied technique among several other control strategies because of their design and implementation simplicity [7].

Despite this advantage, the performance of the PID controller is largely affected by a mismatch in system parameters [8] and associated overshoot, which has led to many approaches, including intelligent algorithms, being used to tune its parameters [9]. Additionally, the PID controller is classified as a linear control system, exhibiting poor anti-interference capabilities and a significant disadvantage in its reliance on manual parameter adjustments. Therefore, several other control techniques are being implemented to address the shortcomings of the classical PID technique.

A Model Reference Adaptive Control-based PID (MRAC-PID) controller was applied in the yaw-axis stabilization of a microsatellite to enhance the settling time in [4]. PID and fuzzy-PID models were used in the SAC system. The PID offered faster steady-state, though there was certain torque oscillation, while the fuzzy-PID provided smoother and improved stability in transient and steady-state performance response [2]. Portella et al. [10] used four control moment gyroscopes (CMGs) pyramidal model to investigate the performance of a circular on-orbit flight satellite. The four CMGs' pyramidal arrangement employs either a linear quadratic tracker (LQT) with an integrator or exponential mapping control (EMC). The results indicated that the LQT has high settling time due to the use of only an integral control algorithm without proportional and derivative schemes. At the same time, the EMC showed faster but more oscillatory performance. PID, adaptive PID, and Fuzzy Logic Control (FLC) were separately compared in a laboratory nanosatellite and its testing system in [11]. The FLC rather than PID yielded significant improvement in energy consumption, convergence time, and robustness following changes in environmental conditions, which were the performance criteria, including steady state error (accuracy). Narkiewicz et al. [12] applied a PID controller whose gains are selectable for a nanosatellite attitude control and stabilization system with a generic model. In using radiation pressure of sum from solar panels with dual-mode Model Predictive Control (MPC), three-axis stabilization control of a spacecraft attitude that is under-actuated with two reaction wheels was achieved in [13]. Using a variable structured PID controller, [14] achieved attitude control of satellites by integrating a conventional PID model, trajectory planning, variable structure, and fault tolerance. The controller was designed to improve the convergence rate of the system. Enejor et al. [15] carried out a performance comparison of the PID control system and Linear Quadratic Regulator (LQR) regarding LEO satellite on-orbit flight stabilization. The study revealed that after 500 seconds, the PID was not able to stabilize the system, contrary to the LQR, which achieved the specifications for the yaw, roll, and pitch-axis. A genetic algorithm (GA) optimized fuzzy logic control system was used for attitude control in a nanosatellite by DelCastañedo et al. [16]. Considering the possible modes along the whole satellite mission, a multi-objective function cost was to optimize the fuzzy controller. Both mono and multi-objective optimizations were carried out. The system performance with mono objective optimization resulted in output that cannot be applied in practice as a result of the enormous cost of electrical power. The multi-objective optimization offered results that permit some rapid flexibility in changing the controller, including at low cost.

From the literature, it was observed that the adaptive PID controller effectively eliminates the oscillatory actions of PID, which were previously caused by initial overshoot. Consequently, the convergence time of the PID was significantly minimized for non-satellite ACS [11]. The high overshoot effect of a PID causes instability in the system's performance and impacts the smoothness of the control process. This underscores the need for a control system that will eliminate high overshoot in the system to ensure smooth and improved stability during the on-orbit flight operation of the satellite. Therefore, taking into account the advantage of an adaptive PID controller, an adaptive control system with a modified PID model (called MRAC-PIDD) and an enhanced FLC algorithm (called AGE-FLC) was proposed in this paper for the LEO satellite yaw-axis ACS. The main objective is to enhance the dynamic response of LEO satellite yaw-axis attitude. The specific objectives are to determine the dynamic equations of the components of satellite yaw-axis ACS, develop control systems based on the algorithms of the proposed solutions, and evaluate the performance of different control systems, including the proposed solution, via simulation tests in MATLAB/Simulink.

2- System Design

The yaw-axis attitude control system is modelled as a closed-loop control system, as shown in Figure 1. The system comprises a controller, an amplifier, a Direct Current (DC) motor, a satellite system, and a feedback sensor with unity gain. The controller regulates a system's behaviour by adjusting inputs to achieve the desired output. Its functions include monitoring the system's state,

comparing the actual output to the desired input, calculating the error, and sending a control signal to adjust the system's input. An amplifier increases the amplitude of a signal. In a feedback control system, it amplifies feedback signals to improve system stability and accuracy. DC motor is an electric motor that converts direct current electrical energy into mechanical energy. In control system, it can be used for position control, speed control, or motion control. In the control system, the feedback sensor measures physical parameters such as position and provides feedback to the controller, thus allowing it to adjust the system's input; and helps detect deviation from the desired set points.

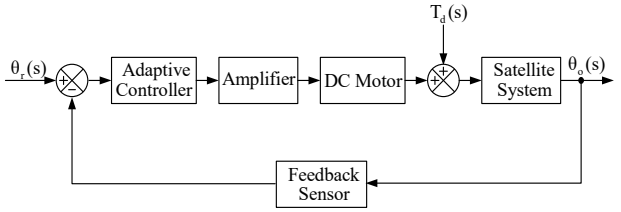

Fig. 1 Closed Loop Network of Satellite Yaw-axis ACS

For the yaw-axis ACS shown in Figure 1, the objective of the design is to ensure that the yaw-axis attitude or angle is stabilized by providing a suitable control manoeuvre that returns and keeps the satellite on its referenced or target attitude. In the figure, $\theta_r(s)$ is the reference or target attitude, while $\theta_o(s)$ is the actual attitude. Hence, to achieve stabilization and effective control of yaw-axis attitude at any instant, $\theta_r(s) = \theta_o(s)$. To meet the design objective, the proposed system is expected to achieve the following design criteria for a typical LEO satellite system: overshoot of ≤ 5%, settling time of ≤ 10 seconds, and zero steady-state error [1],[15].

2-1- Mathematical Modelling

For the closed-loop control system shown in Figure 1, the closed-loop model for the yaw-axis ACS, neglecting the controller, consists of the amplifier, DC motor, and satellite structure components. The mathematical models of these components, which comprise the amplifier, DC motor, and satellite structure, are derived subsequently.

2-1-1- Mathematical Model of Amplifier

The dynamic equation of the amplifier with gain k_a is defined in terms of the output voltage by [1]:

$$V_a(s) = K_a V_i(s) \tag{1}$$

where $V_a(s)$ is the amplifier voltage, K_a is the amplifier gain, and $V_i(s)$ is the input voltage.

Hence, the open-loop gain of the amplifier can be expressed by Eq. (2).

$$K_a = \frac{V_a(s)}{V_i(s)} \tag{2}$$

2-1-2- Mathematical Model of DC Motor

An armature-controlled DC motor is schematically represented in Figure 2. In the figure, DC motor is shown to have armature resistance and inductance R_a and L_a respectively, input or armature voltage, V_a , armature current I_a , and motor back electromotive force (EMF) of V_b that make up the electrical component of the motor. The mechanical components are the motor moment of inertia J_a , damping ratio of the motor B_a, and the motor shaft angular position $\theta(t)$.

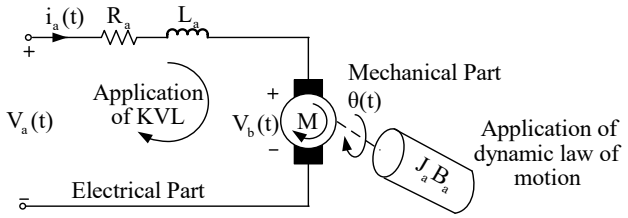

Fig. 2 Schematic Diagram or Armature Controlled DC Motor

Kirchhoff's voltage law (KVL) and dynamic law of motion application in the electrical and mechanical parts of the DC motor results to Eq. (3), Eq. (4), and Eq. (5) as seen in [17],[18].

$$V_a(t) = R_a I_a(t) + L_a \frac{dI_a(t)}{dt} + V_b(t) \tag{3}$$

$$V_b(t) = K_b \omega_m(t) = K_b \frac{d\theta(t)}{dt} \tag{4}$$

$$T_m = K_m I_a \tag{5}$$

where ω_m is the motor angular speed and is equal to the derivation of the motor angular position or displacement, K_b is the motor back EMF constant, T_m is the motor toque, and K_m is the torque constant of the motor. Eq. (5) can further be expressed by Eq. (6).

$$T_m = J_a \frac{d^2\theta(t)}{dt} + B_a \frac{d\theta(t)}{dt} \tag{6}$$

By substituting Eq. (4) into Eq. (3), Eq. (5), and Eq. (6), Eq. (7) and (8) are established.

$$V_a(t) = R_a I_a(t) + L_a \frac{dI_a(t)}{dt} + K_b \frac{d\theta(t)}{dt} \quad (7)$$

$$J_a \frac{d^2\theta(t)}{dt} + B_a \frac{d\theta(t)}{dt} = K_m I_a \quad (8)$$

Taking the Laplace transform of Eq. (7) and Eq. (8), and assuming zero initial conditions gives Eq. (9) and Eq. (10).

$$V_a(s) = L_a s I_a(s) + R_a I_a(s) + K_b s\theta(s) \quad (9)$$

$$J_a s^2\theta(s) + B_a s\theta(s) = K_m I_a(s) \quad (10)$$

By equating Eq. (9) and Eq. (10), the armature current was eliminated leading to the formulation presented in Eq. (11).

$$\frac{V_a(s) - K_b s\theta(s)}{sL_a + R_a} = \frac{J_a s^2\theta(s) + B_a s\theta(s)}{K_m} \quad (11)$$

The constants K_b and K_m are usually given as $K_b = K_m = K$ in most DC motor [1]. Therefore, Eq. (11) can be expressed in terms of transfer function as the ratio of the motor angular position to the armature input voltage as presented in Eq. (12).

$$\frac{\theta(s)}{V_a(s)} = \frac{K}{s[(J_a s + B_a)(L_a s + R_a) + K^2]} \quad (12)$$

2-1-3- Mathematical Model of Satellite System

The load torque (T_L) due to the torque delivered by the DC motor (T_m) and the disturbance torque (T_d) as shown in Figure 1 is given by Eq. (13).

$$T_L = T_m + T_d \quad (13)$$

The moment of inertia J of the entire system consists of the motor moment of inertia J_a and the moment of inertia of the satellite structure or body J_l about axis of rotation at the center of mass [1]. Given the associated vicious friction B of the satellite structure (i.e. the load) and its actual angular position $\theta_a(t)$ about the yaw-axis, the load (satellite) torque assuming $T_d = 0$ is given by Eq. (14):

$$T_L = T_m = J \frac{d^2\theta_o(t)}{dt} + B \frac{d\theta_o(t)}{dt} \quad (14)$$

The Laplace transform of Eq. (14) assuming zero initial condition, is given by Eq. (15).

$$T_m(s) = Js^2\theta_0(s) + Bs\theta_0(s) \quad (15)$$

The transfer function describing the satellite's body dynamics, specifically the relationship between the actual angular position or attitude of the yaw-axis and the input motor torque $T_m(s)$, is provided in Eq. (16).

$$\frac{\theta_o(s)}{T_m(s)} = \frac{1}{s(Js + B)} \quad (16)$$

Table 1 shows the description of the values of the physical parameters for amplifier, DC motor, and satellite structure of Low Earth Satellite (LEO).

Table 1: Parameters of the Yaw-axis ACS [1]

Definition	Symbol	Value
Amplifier	K_a	10
Motor a constant	K	0.01 Nm/A
Resistance of motor	R_a	1 Ω
Inductance of motor	L_a	0.5 H
Damping ratio of motor	B_a	0.01 Kgm^2
Moment of inertia of motor	J_a	0.1 Nms
Moment of inertia of satellite	J	2.5 Kg m^2
Damping ratio of satellite	B	1.17 Nms

Substituting the values for the parameters in Table 1 into Eq. (2), Eq. (12), and Eq. (16) yields the numerical expressions for amplifier transfer function gain, the DC motor transfer function, and the satellite body transfer function as presented in Eq. (17), Eq. (18), and Eq. (19), respectively.

$$\frac{V_a(s)}{V_i(s)} = 10 \quad (17)$$

$$\frac{\theta(s)}{V_a(s)} = \frac{0.01}{0.05s^3 + 0.105s^2 + 0.0101s} = \frac{0.2}{s^3 + 2.1s^2 + 0.202s} \quad (18)$$

$$\frac{\theta_o(s)}{T_m(s)} = \frac{1}{2.5s^2 + 1.17s} \quad (19)$$

The yaw-axis ACS is represented with a block diagram in terms of the transfer function of the amplifier, DC motor, satellite body, and unity gain feedback sensor, assuming zero torque disturbance, in Figure 3.

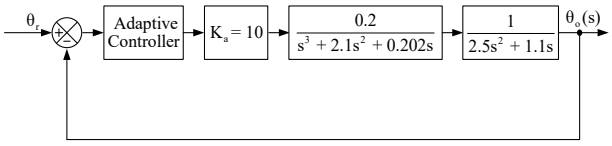

Fig. 3 Closed Loop Network of Satellite Yaw-axis ACS with Zero Torque Disturbance

2-2- Design of MRAC Based PIDD Controller

The yaw-axis ACS for LEO satellite is achieved by designing an MRAC based PIDD controller. In designing MRAC, many approaches such as Massachusetts Institute of Technology (MIT) rule, augmented error theory, and Lyapunov theory can be used. Nevertheless, approach based on MIT is used in this work. In designing a MRAC, it is required that the error and cost function be determined as shown as part of this subsection. Figure 4 is the proposed MRAC based PIDD controller for yaw-axis attitude determination.

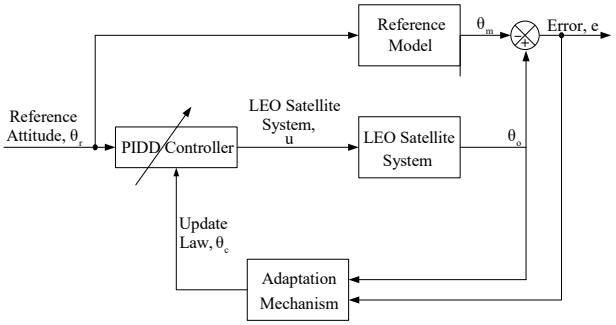

Fig. 4 The Proposed MRAC-PIDD Control System for LEO Satellite Yaw-axis ACS

2-2-1- Update Law Mechanism

The update law or the adjustment mechanism is achieved from the following mathematical expressions defined as follows.

In starting the development of the adaptation mechanism that governs the update law, the deviation (or error) due to the difference of the plant response θ_o and the output $\theta_{\mathrm{mod}\,el}$ of the reference model is expressed as in Eq. (20).

$$\text{Error, } e = \theta_o - \theta_m \tag{20}$$

The cost function $J_g(\theta_c)$ is defined in Eq. (21) in terms of *e* as;

$$J_g(\theta_c) = \frac{1}{2}e^2 \tag{21}$$

The cost function is minimized such that θ_c can be sustained in negative gradient direction of J_g defined by Eq. (22).

$$\frac{d\theta_c}{dt} = -\gamma \frac{\partial J}{\partial \theta_c} = -\gamma e \frac{\partial e}{\partial \theta_c} \tag{22}$$

The change in θ_c is established by Eq. (22) with respect to time so as the cost function can be minimized to zero. Also, $\partial e/\partial \theta_c$ is regarded as the sensitivity derivative [19]. It shows the error change with respect to the gain, which is a quantity of positive value for the controller's adaptation mechanism [20],[21]. A reference model, whose performance characteristic the satellite positioning system is to follow, is established next, and this forms the design objective of the MRAC.

Assuming the system transfer function is defined as $KG_p(s)$ where K is a quantity of unknown value and $G_p(s)$ represents transfer function of the plant. Let an expression be defined for the reference model as presented in Eq. (23).

$$G_m(s) = K_o G_p(s) \tag{23}$$

where K_o is a quantity of known value. Eq. (20) can be redefined resulting to Eq. (24).

$$E(s) = KG_p(s)U(s) - K_o G_p(s)U_c(s) \tag{24}$$

where $KG_p(s)U(s) = \theta_o$, $U(s)$ is the control input to the plant, $K_o G_p(s)U_c(s) = \theta_m$ and $U_c(s)$ the reference model input.

Thus, Eq. (25) defines the control law:

$$U(s) = \theta_c \times U_c(s) \tag{25}$$

By substituting Eq. (24) into Eq. (23), a partial derivative is applied with the resulting expression defined by Eq. (26)

$$\frac{\partial E(s)}{\partial \theta_c} = KG_p(s)U_c(s) = \frac{K}{K_o}\theta_m \tag{26}$$

Equating Eq. (22) and Eq. (26) gives Eq. (27)

$$\frac{d\theta_c}{dt} = -\gamma e \frac{K}{K_o}\theta_m = -\gamma^1 e \theta_m \tag{27}$$

where $\gamma^1 = \gamma K/K_o$ and the update law is represented by Eq. (27).

2-2-2- Determination of the Reference Model

For an MRAC, it is usually required to define a reference model $G_m(s)$. Since the satellite structure is a second-order model, in this work, the performance of the entire model of the satellite system is constrained to that of a second-order reference model dynamic and steady-state that will meet the stated performance specifications or criteria for the yaw-axis ACS. Hence, Eq. (28) defines the reference model:

$$G_m(s) = \frac{\omega_n^2}{s^2 + 2\zeta\varpi_n s + \omega_n^2} \quad (28)$$

where ω_n is the system natural frequency and ζ is the system damping ratio. The determination of the values for these quantities is carried out with Eq. (29).

$$O_p = e^{-\pi\zeta/\sqrt{1-\zeta^2}} \quad (29)$$

where O_p is the peak percentage overshoot of value 2%. Solving Eq. (29) gives Eq. (30).

$$\log_e\left(\frac{5}{100}\right) = -\frac{\pi\zeta}{\sqrt{1-\zeta^2}}\log_e^e \quad (30)$$

This results in $\zeta = 0.78$. With the value of the damping ratio determined, the natural frequency of the system is determined using Eq. (31).

$$T_s = \frac{4}{\zeta\omega_n} \quad (31)$$

Thus $\omega_n = 5.13\ \text{rads}^{-1}$, Substituting this value into Eq. (28) gives Eq. (32).

$$G_m(s) = \frac{26.32}{s^2 + 8s + 26.32} \quad (32)$$

Eq. (32) is the designed referenced model.

2-2-3- Design of PID and PIDD Controllers

Figure 5 shows a simplified structure of PID control system used to achieve three-term process control.

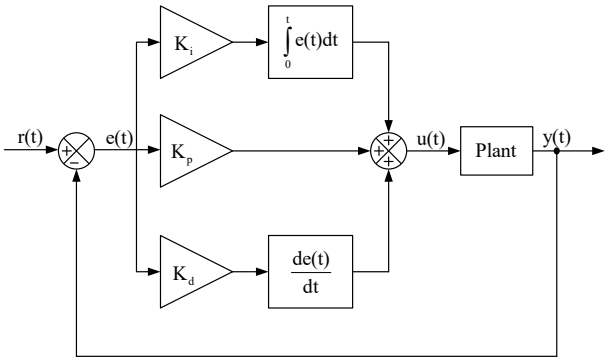

Fig. 5 PID Control System Representation

The mathematical expression of PID controller can be determined by analyzing Figure 5. Hence, $r(t)$, $e(t)$, and $u(t)$ represents the desired input, error and the control command. Furthermore, K_p, K_i, K_d are the gains of the PID controller: proportional gain, integral gain, and derivative gain. The output $y(t)$ is related to $r(t)$ by Eq. (33).

$$e(t) = r(t) - y(t) \quad (33)$$

The proportional, integral and derivative computation carried on the error as it is fed into the PID controller results to a control action given by Eq. (34).

$$u(t) = K_p e(t) + K_i\int_0^t e(t)dt + K_d\frac{de(t)}{dt} \quad (34)$$

Eq. (34) is a PID control variable in time domain. Thus, the Laplace transform of PID control variable assuming zero initial condition is given by Eq. (35).

$$U(s) = K_p E(s) + K_i\frac{1}{s}E(s) + K_d sE(s) \quad (35)$$

Or in a more simplified form as presented in Eq. (36):

$$C(s) = K_p + K_i\frac{1}{s} + K_d s \quad (36)$$

where, $C(s) = U(s)/E(s)$ and is the PID controller. The gains of the PID controller obtained by tuning the

MATLAB/Simulink PID block are [specific gains]. Thus, the designed PID controller is given by Eq. (37).

$$C(s) = 1.98 + \frac{0.0215}{s} + 1.85s \quad (37)$$

PID controllers typically introduce overshoot in control systems, which is addressed by adding an extra *D* element in this work. Hence, PIDD is a modified PID controller with extra *D* element and it is given by [22]:

$$C(s) = K_p + K_i\frac{1}{s} + K_{d1}s + K_{d2}s^2 \quad (38)$$

where $C(s) = U(s)/E(s)$ and is the PID controller. The gains of the PID controller obtained by tuning the MATLAB/Simulink PID block are [specific gains]. Therefore, the designed PIDD controller is given by Eq. (39):

$$C(s) = 1.98 + \frac{0.0115}{s} + 1.85s + 1.85s^2 \quad (39)$$

2-3- Design of Fuzzy Logic Controller

In designing an FLC, the components involved are fuzzification, defuzzification, rule base, and interference mechanism. Decision making is performed by the interference mechanism. Figure 6 is a block diagram of fuzzy logic control of satellite yaw-axis ACS.

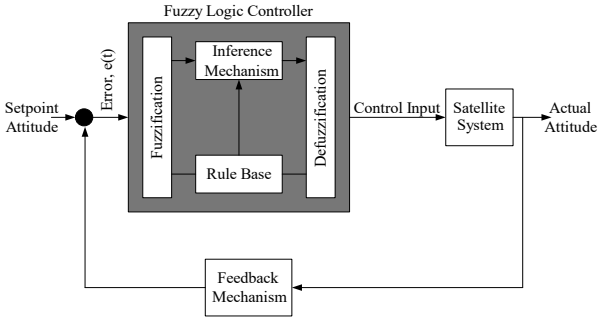

Fig. 6 Fuzzy Control System Representation

Fuzzification is performed, which involves transforming a crisp fuzzy input set into linguistic variables. The input sets or variables in this case are the error E and the change in error (ΔE). Proper scaling factors were used to scale the error and change in error for the yaw-axis attitude. The resulting linguistic variables from the fuzzification are negative big (NB), negative medium, negative small (NS), zero (ZO), positive small (PS), positive medium (PM), and positive big (PB). The corresponding fuzzy logic control rule table is shown in Table 2. For the designed FLC, each input has 3 membership functions (MFs) while the output has 5 MFs.

Table 2: Rule Base Table of the FLC

E/ΔE	NE	ZO	PO
NE	NB	NM	ZO
ZO	NM	ZO	PM
PO	ZO	PM	PB

The designed FLC was realized using the Mamdani model in MATLAB/Simulink environment. Centroid was used for the purpose of defuzzification. The inputs and outputs were modelled using the triangular MF. The resulting shapes of the triangular MFs are shown in Figure 7. The Simulink model for the designed FLC control system is shown in Figure 8. The output of the developed fuzzy model was enhanced by an adjustable gain to improve its performance as in [6]. This is called Adjustable Gain Enhanced FLC (AGE-FLC).

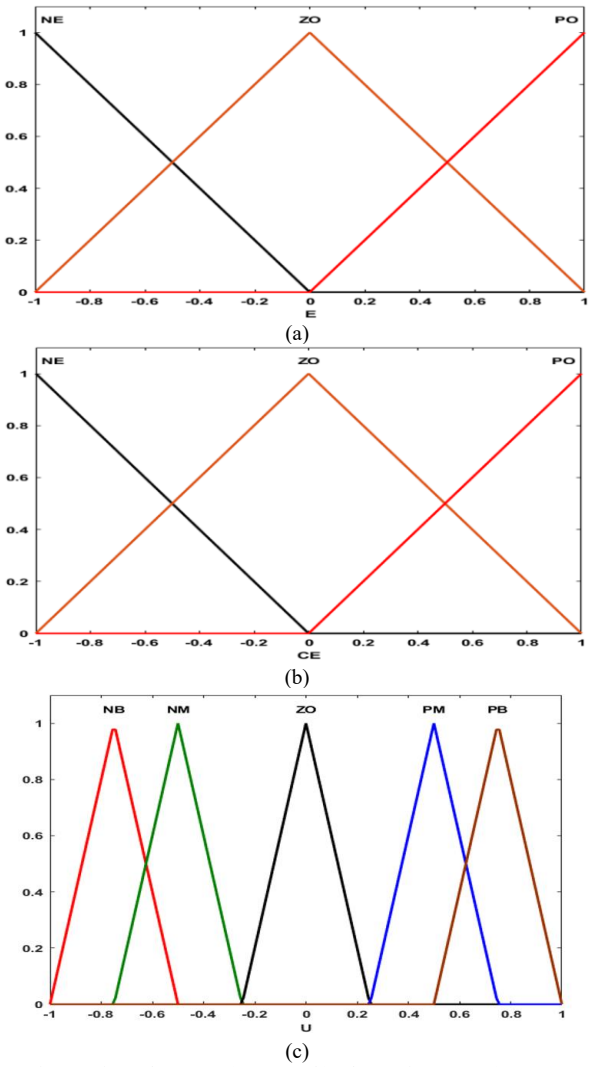

Fig. 7 Triangular MFs: (a) Error (b) Change in Error (c) Output

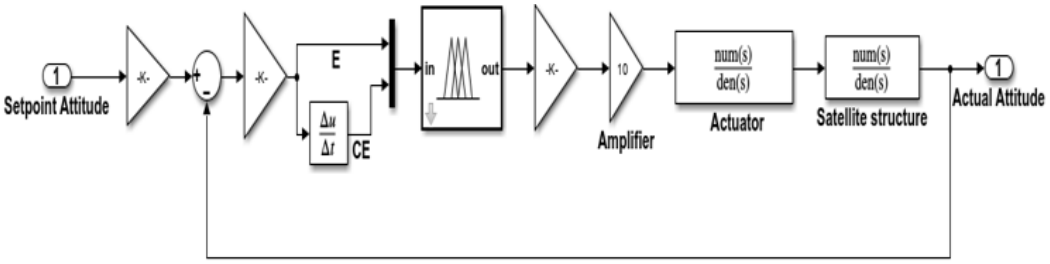

Fig. 8 Simulink Model of the Fuzzy Logic Controlled ACS

3- Results and Discussion

3-1- Analysis of the System without Controller

In this scenario, simulation analysis was conducted to investigate the performance of the microsatellite yaw axis attitude in the absence of a controller. That is no controller was introduced as a subsystem in the attitude control system (ACS) so as to ensure the stabilization of the satellite yaw angle and tracked the desired yaw-axis attitude while ensuring that the system performance criteria that include rapid convergence (that is reaching steady state as fast as possible, which is defined by the settling time in second) with little or no cycling (defined in terms of peak overshoot in percentage) are met. The resulting step response of the uncompensated satellite yaw-axis ACS (Sys1) is shown in Figure 9. The numerical analysis of the step response curve is shown in Table 3.

Table 3: Time Domain Characteristics of System Without Controller

Step Response Parameter	Value
Rise time	2.17 s
Transient time	22.14 s
Settling time	22.14 s
Peak overshoot	38.66%
Final value	0.89
Steady state error	0.11

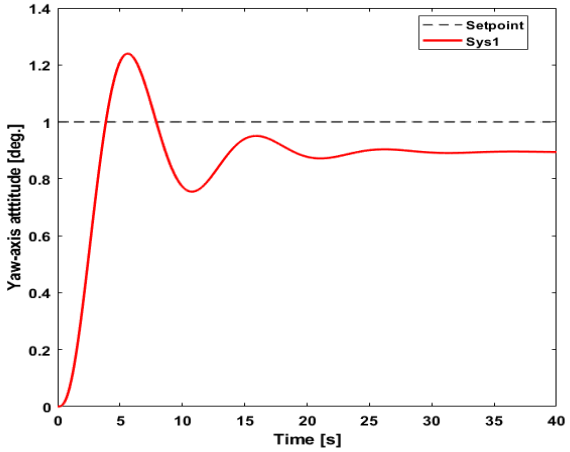

Fig. 9 Step Response of System without a Controller

Considering the step response shown in Figure 9, the numerical analysis as shown in Table 3 revealed that in the absence of a control algorithm, the system has a transient and steady-state that is characterized by rise time of 2.17 seconds, transient time and settling time 22.14 seconds respectively, peak overshoot of 38.66%, final value of 0.89 degree, and steady state error of 0.11. As shown in Figure 9, the curve reveals that in the absence of a controller, the system fails to achieve the desired attitude and suffers from high instability, which can be attributed to the magnitude or size of the overshoot. Therefore, there is a need to design a controller for on-orbit flight performance improvement in terms of yaw angle stability with significantly reduced overshoot or zero overshoot.

3-2- Analysis of PID/PIDD Control System

The simulation analysis of the PID and the PIDD controllers applied to the LEO satellite yaw axis attitude control system is presented in this section. Figure 10 shows the step response curves of the PID and the PIDD controllers. Table 4 shows the numerical analysis of the performance of the control system scenario considered using PID or PIDD controllers.

Table 4: Time Domain Characteristics of PID/PIDD

Step Response Parameter	PID	PIDD
Rise time (s)	1.93	4.26
Transient time (s)	7.97	8.34
Settling time (s)	7.97	8.34
Peak overshoot (%)	12.00	0.00
Final value	1.00	1.00
Steady state error	0.00	0.00

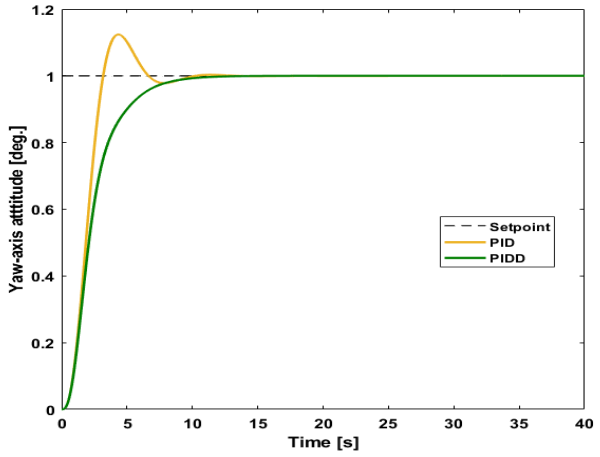

Fig. 10 Step Response of PID/PIDD Control System

Looking at Figure 10 and Table 4, it can be deduced that the PID control system showed better performance in terms of rise time and settling time than the PIDD control system. However, in terms of overshoot (or stability performance), the PIDD controller outperformed the PID controller. Though the PID control system showed good performance in terms of rise time and settling time, it did not meet all the performance criteria required of the control system, specifically the overshoot, which is 12% (i.e. > 5%). On the other hand, the PIDD control system meets the designed requirement for both settling time and overshoot: 8.34 seconds (i.e. < 10 seconds) and 0.01% (i.e. < 5%).

3-3- Analysis of the MRAC-PID/MRAC-PIDD Control System

The performances of the adaptive PID and the adaptive PIDD control systems used for the control of the yaw-axis attitude of the LEO satellite are presented in this subsection. The step response curves and the table of the numerical values obtained from the simulation analysis conducted in MATLAB/Simulink environment with respect to the designed MRAC-PID and MRAC-PIDD yaw-axis ACS for LEO satellite are presented in Figure 11 and Table 5.

Table 5: Time Domain Characteristics of MRAC Based Control System

Step Response Parameter	MRAC-PID	MRAC-PIDD
Rise time (s)	1.74	4.28
Transient time (s)	6.19	8.95
Settling time (s)	6.19	8.95
Peak overshoot (%)	3.94	0.00
Final value	1.00	1.00
Steady state error	0.00	0.00

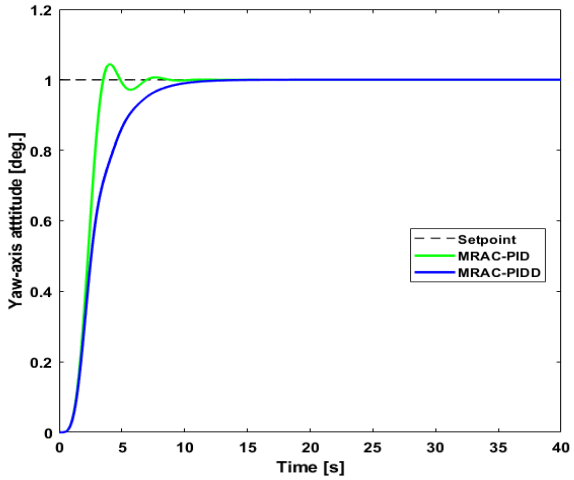

Fig. 11 Step response of MRAC-PID/MRAC-PIDD Control System

The step response curves in Figure 11 revealed that the MRAC-PID still exhibits slight oscillation though the design or performance criteria was achieved by both control systems. As shown in Table 5, the MRAC-PID yielded faster response and better convergence time in terms of rise time and settling time than the MRAC-PIDD. However, the MRAC-PIDD showed more smooth and stable performance than the MRAC-PID, which is an indication of better control torque during the operation of the satellite [2].

3-4- Analysis of Fuzzy Logic Control System

The performances of the developed FLC and its enhanced type (AGE-FLC) are presented in Figure 12 and Table 6. The simulation curves in Figure 12 reveal the step response performance of the FLC and the AGE-FLC with the gain K varied between $0.70 \leq K \leq 0.90$ for optimal response efficiency.

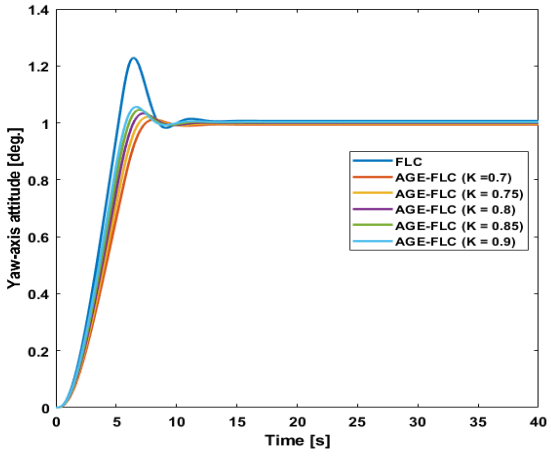

Fig. 12: Step Response of FLC/AGE-FLC Control System

Table 6: Time Domain Characteristics of FLC Based Control System

Step Response Parameter	FLC	AGE-FLC (K = 0.7)	AGE-FLC (K = 0.75)	AGE-FLC (K = 0.8)	AGE-FLC (K = 0.85)	AGE-FLC (K = 0.9)
Rise time (s)	3.33	4.50	4.23	4.26	3.81	3.64
Transient time (s)	9.52	7.01	8.18	8.32	7.87	7.67
Settling time (s)	9.52	7.01	8.18	8.32	7.87	7.67
Peak overshoot (%)	21.97	1.73	2.51	0.00	4.43	5.23
Final value	1.00	1.00	1.00	1.00	1.00	1.00
Steady state error	0.00	0.00	0.00	0.00	0.00	0.00

As shown in Figure 12 and Table 6, the FLC showed the best performance in terms of rise time, but give the worst performance with respect to settling time and overshoot. Among the AGE-FLCs, it can be seen that all met the performance criteria stated for the LEO satellite except when the gain was equal to 0.9. Thus, for optimal performance using the developed AGE-FLC for the LEO satellite yaw-axis ACS, the adjustable gain should be tuned between 0.7 and 0.85. Since stability is of utmost priority for orbiting satellites in space, the best performance is offered by AGE-FLC when K = 0.8 because it offers an overshoot of zero. It also offered smoother and more stable torque control performance [2]. Hence, amongst the AGE-FLCs, the method for K = 0.8 was used for comparison with other control systems implemented for the LEO satellite yaw-axis ACS.

3-5- Performance Comparison of Control Systems

In this section, the various control schemes implemented were compared as by the step response of the yaw-axis attitude in degree shown in Figure 13.

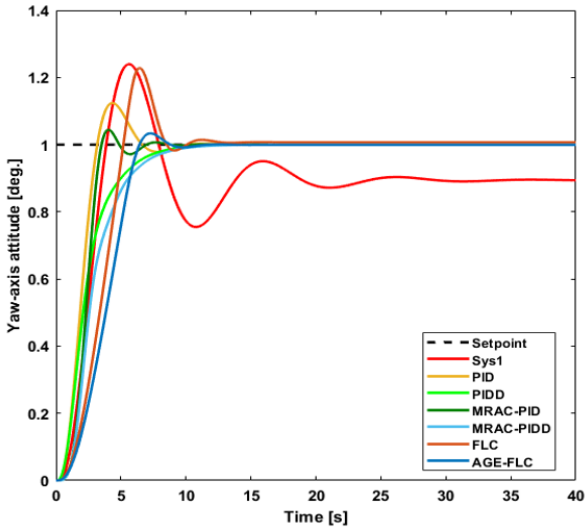

Fig. 13 Step response comparison of control systems

Among the control systems, the FLC shows the worst performance in terms of settling time and overshoot. Also, of all the control systems, only the PID and the FLC controllers did not meet the stated performance criteria considering their overshoots. The MRAC-PID controller offered the fastest response (in terms of rise time) and fastest transient time (settling time) compared to other control strategies. Thus, MRAC-PID provides the shortest time reach stability compare to other controllers. However, the MRAC-PID has an overshoot associated with its response. On the other hand, using the PIDD, MRAC-PIDD, or the AGE-FLC (K = 0.8) control system revealed that each of them effectively prevents oscillation or fluctuation of the control torque, considering the no overshoot they offered [2]. Hence, by this performance, the PIDD, MRAC-PIDD, and the AGE-FLC control systems provided the best performance in smoothness and stability.

Now, considering the settling times and overshoots of the PIDD, MRAC-PIDD, and the AGE-FLC with respect to the performance criteria established, it suffices to say that AGE-FLC provided the best performance by providing the fastest transition to stable state (steady-state) with no fluctuation in torque control handling. Generally, in terms of overall performance for meeting the stated design or performance criteria: overshoot of less than or equal to 5% and settling time of less than or equal to 10 seconds, the adaptive PID controller outperformed both the conventional PID and FLC controllers. This agrees with the experimental observation wherein adaptive PID offered the most performance compared to conventional PID and FLC for nanosatellite ACS in [11].

4- Conclusions

In this paper, adaptive controllers (MRAC-PID and MRAC-PIDD) and AGE-FLC have been developed for LEO satellite yaw-axis attitude control system (ACS). For the objective of the study to be achieved, the dynamic equations describing the yaw-axis attitude of a LEO satellite were derived. The dynamic equations were then modelled using Simulink embedded blocks in MATLAB. Each of the model components shows different features of Simulink, including transfer function block, gain block, PID block, and fuzzy logic block. MRAC-based PID/PIDD controllers and an AGE-FLC were developed.

The designed control systems were modelled and simulated in the MATLAB/Simulink environment. The results from the simulation revealed that the proposed controllers met the performance specifications of the LEO satellite yaw-axis ACS, given as overshoot of $\leq 5\%$ and settling time of ≤ 10 seconds and zero steady-state error. Notably, the MRAC-PIDD and the AGE-FLC provided negligible overshoot. This indicated that stabilization was effectively achieved and both controllers offered smoothness in control torque during the satellite operation. Generally, considering the time domain characteristic of the system response without a controller, it suffices to say that the introduction of the designed adaptive PID/PIDD controllers and the AGE-FLC largely enhanced the system performance by offering settling time less than 10 seconds and overshoot very much less than 5%. Thus, the proposed controllers met the design criteria for a typical LEO satellite system. In future work, it is recommended to integrate the PID algorithm with the FLC. Other intelligent control techniques, such as swarm algorithms or machine learning models, can be implemented with PID to reduce the settling time further. Other control system scenarios should be studied regarding the evaluation of the control systems with disturbance torque.

References

[1] C. C. Mbaocha, C. U. Eze, I. A. Ezenugu, and J. Onwumere, "Satellite Model for Yaw-axis Determination and Control using PID Compensator," International Journal of Scientific & Engineering Research, Vol. 7, No. 7, 2016, pp. 1623-1629.

[2] Y. Shan, L. Xia, and S. Li, "Design and Simulation of Satellite Attitude Control Algorithm Based on PID," Journal of Physics: Conference Series, Vol. 2355, No. 012035, 2022. pp. 1-9.

[3] H. Travis, "Introduction to Satellite Attitude Control," In Advances in Spacecraft Attitude Control, IntechOpen. 2020.

[4] P. C. Eze, and I. A. Ezenugu, "Microsatellite Yaw-axis Attitude Control System using Model Reference Adaptive Control Based PID Controller, "International Journal of Electrical and Control Engineering Research, Vol. 4, No. 2, 2024, pp. 8-16.

[5] A. T. Ajiboye, J. O. Popoola, O. Oniyide, and S. L. Ayinia, "PID Controller for Microsatellite Yaw-axis Attitude Control System Using ITAE Method," TELKOMNIKA Telecommunication, Computing, Electronics and Control, Vol. 18, No. 2, 2020, pp. 1001 – 1011.

[6] P. C. Eze, B. O. Ekengwu, N. C. Asiegbu, and T. I. Ozue, "Adjustable Gain Enhanced Fuzzy Logic Controller for Optimal Wheel Slip Ratio Tracking in Hard Braking Control System," Advances in Electrical and Electronic Engineering, Vol. 19, No. 3, 2021, pp. 231 – 242.

[7] P. C. Eze, A. E. Jonathan, B. C. Agwah, and E. A. Okoronkwo, "Improving the Performance Response of Mobile Satellite Dish Antenna Network within Nigeria," Journal of Electrical Engineering, Electronics, Control and Computer Science, Vol. 6, No. 21, 2020, pp. 25-30.

[8] B. C. Agwah, and P. C. Eze, "An Intelligent Controller Augmented with Variable Zero Lag Compensation for Antilock Braking System," International Journal of Mechanical and Mechatronics Engineering, Vol. 6, No. 11, 2022, pp. 303-210.

[9] P. C. Eze, J. K. Obichere, E. S. Mbonu, and O. J. Ononjo, "Positioning Control of Satellite Antenna for High Speed Response Performance," IPTEK, The Journal of Engineering, Vol. 10, No. 2, 2024, pp. 119-136.

[10] K. M. Portella, W. N. Schinestzki, R. M. Sehnem, L. B. da Luz, L. Q. Mantovani, R. R. Sacco, S. S. Kraemer, and P. Paglione, "Satellite Attitude Control Using Control Moment Gyroscopes," Journal of Aerospace Technology and Management, São José dos Campos, Vol. 12, 2020, pp. 94-105.

[11] A. Bello, K. S. Olfe, J. Rodríguez, J. M. Ezquerro, and V. Lapuerta, "Experimental Verification and Comparison of Fuzzy and PID Controllers for Attitude Control of Nanosatellites," Advances in Space Research, Vol. 71, 2023, pp. 3613-3630.

[12] J. Narkiewicz, M. Sochacki, and B. Zakrzewski, "Generic model of a satellite attitude control system. International Journal of Aerospace Engineering," Vol. 2020, pp. 1-17.

[13] L. Jin, and Y. Li, "Model Predictive Control-based Attitude Control of Under Actuated spacecraft Using Solar Radiation Pressure," Aerospace, Vol. 9, 2022, pp. 1-20.

[14] Y. Qi, H. Jing, and X. Wu, "Variable structure PID Controller for Satellite Attitude Control Considering Actuator Failure," Applied Sciences, Vol. 12, 2022, pp. 1-19.

[15] E. U. Enejor, F. M. Dahunsi, K. F. Akingbade, and I. O. Nelson, "Low Earth Orbit Satellite Attitude Stabilization Using Linear Quadratic Regulator," European Journal of Electrical and Computer Science, Vol. 7, No. 3, 2023, pp. 17 – 29.

[16] Á. del Castañedo, D. Calvo, Á. Bello, and M. V. Lapuerta, "Optimization of Fuzzy Attitude Control for Nanosatellites," In: K. Arai, S. Kapoor, R. Bhatia (eds) Intelligent Systems and Applications. InelliSys 2018. Advances in Intelligent Systems and Computing, Vol 869. Springer, Cham.

[17] P. C. Eze, C. A. Ugo, and D. S. Inaibo, "Positioning Control of DC Servomotor-based Antenna using PID Tuned Compensator," Journal of Engineering Sciences, Vol. 8, No. 1, 2021, pp. E9-E16.

[18] I. O. Akwukwaegbu, O. C. Nosiri, M. Olubiwe, C. F. Paulinus-Nwammuo, and E. Okonkwo, "Design of Model Following Control Integrating PID Controller for DC Servomotor-based Antenna Positioning System," SSRG International Journal of Electrical and Electronics Engineering, Vol. 10, No. 6, 2023, pp. 33-42.

[19] P. C. Eze, D. O. Njoku, O. C. Nwokonkwo, C. G. Onukwugha, J. N. Odii, and J. E. Jibiri, "Wheel Slip Equilibrium Point Model Reference Adaptive Control Based PID Controller for Antilock Braking System: A New Approach," International Journal of automotive and mechanical Engineering, Vol. 21, No 3, 2024, pp. 11581-11595.

[20] P. C. Eze, C. A. Ugoh, C. P. Ezeabasili, B. O. Ekengwu, and L. E. Aghoghovbia, "Servor Position Control in Hard Disk Drive of a Computer Using MRAC Integrating PID Algorithm," American Journal of Science, Engineering and Technology, Vol. 2, No. 4, 2017, pp. 97-105.

[21] A. Daiifarshchi, and S. Bargandan, “Design of a Model Reference Adaptive Controller Using Modified MIT Rule for a Second Order System,” Journal of Artificial Intelligence in Electrical Engineering, Vol. 7, No. 25, 2018, pp. 7-14.

[22] M. A. Fawwaz, K. Bingi, R. Ibrahim, P. A. M. Devan, and B. R. Prusty, "Design of PIDD Controller for Robust Performance of Process Plants," Algorithms, Vol. 16, 2023, pp. 437